Heterogeneously-Grown Tunable Group-IV Laser on Silicon

Mantu Hudait*[a], M. Clavel[a], L. Lester[a], D. Saladukha[b,c], T. Ochalski[b,c], and F. Murphy-Armando[b,c]
[a]Bradley Department of Electrical and Computer Engineering, Virginia Tech, Blacksburg, VA, USA 24061; [b]Tyndall National Institute, Lee Maltings, Dyke Parade, Cork, Ireland; [c]Centre for Advanced Photonics and Process Analysis, Cork Institute of Technology, Cork, Ireland

ABSTRACT

Tunable tensile-strained germanium (ε-Ge) thin films on GaAs and heterogeneously integrated on silicon (Si) have been demonstrated using graded III-V buffer architectures grown by molecular beam epitaxy (MBE). ε-Ge epilayers with tunable strain from 0% to 1.95% on GaAs and 0% to 1.11% on Si were realized utilizing MBE. The detailed structural, morphological, band alignment and optical properties of these highly tensile-strained Ge materials were characterized to establish a pathway for wavelength-tunable laser emission from 1.55 μm to 2.1 μm. High-resolution X-ray analysis confirmed pseudomorphic ε-Ge epitaxy in which the amount of strain varied linearly as a function of indium alloy composition in the $In_xGa_{1-x}As$ buffer. Cross-sectional transmission electron microscopic analysis demonstrated a sharp heterointerface between the ε-Ge and the $In_xGa_{1-x}As$ layer and confirmed the strain state of the ε-Ge epilayer. Low-temperature micro-photoluminescence measurements confirmed both direct and indirect bandgap radiative recombination between the Γ and L valleys of Ge to the light-hole valence band, with L-lh bandgaps of 0.68 eV and 0.65 eV demonstrated for the 0.82% and 1.11% ε-Ge on Si, respectively. The highly ε-Ge exhibited a direct bandgap, and wavelength-tunable emission was observed for all samples on both GaAs and Si. Successful heterogeneous integration of tunable ε-Ge quantum wells on Si paves the way for the implementation of monolithic heterogeneous devices on Si.

Keywords: Tensile strain, Ge, InGaAs, MBE, laser, heterogeneous

1. INTRODUCTION

The shrinking feature size of Si transistors has enabled an exponential increase in transistor density, resulting in increased compute power. However, current Si-based complimentary metal-oxide-semiconductor (CMOS) technology is nearing the physical limits of its scaling potential, and with the end in sight of the traditional technology roadmap [1], only a radical departure from Si-based technologies can ensure continued technological progress [2]. New material innovations [3-5], novel device architectures [6-9], heterogeneous technology co-integration [10], new functionalities [11], and their monolithic integration onto Si are projected to continue transistor miniaturization beyond the Si CMOS era. Moreover, interconnect bottlenecks for both inter-chip and intra-chip communication are projected to be major impediments to energy-efficient performance scaling. Therefore, there is an urgent need for large bandwidth, low-resistance interconnects in high-end computing applications as copper-based electrical interconnects are rapidly becoming inefficient in meeting essential bandwidth requirements [12]. It will become increasingly challenging to transmit signals electrically while maintaining low power consumption, low delay, and a high signal-to-noise ratio [13]. An enticing alternative would be the integration of photonic devices with Si technology, hence the monolithic integration of Si-based optoelectronics would be an obvious choice. However, the indirect bandgap of Si limits the realization of Si-based photonic devices [14]. A monolithic integrated laser source on Si has been considered a "holy-grail", since the indirect band gap semiconductors, Si and Ge, are usually regarded unsuitable for laser diodes due to their inefficient radiative recombination. Extensive research has been conducted on porous Si [15], Si nanocrystals [16], ultrathin Si quantum wells (QWs) [17], Si and SiGe nanostructures [18], GeSn [19], Si Raman lasers [20], and III-V lasers grown on [21] or bonded to Si [22]. While stimulated emission from ultrathin Si QWs has been observed, the gain is not enough to overcome losses and enable lasing [23]. Thus, the hybrid integration of Ge and III-V materials-based optoelectronic devices with traditional Si CMOS technology would revolutionize technology needs in the near future. The superior transport properties and large modulation bandwidth of Ge and III-V compound semiconductor material systems make them ideal candidates for integration on Si [24-30]. Figure 1 shows the band structures for unstrained and strain-engineered Ge, illustrating the possibility of enhanced light emission through strain engineering [31]. Besides, Ge-based light sources on Si are important for the realization of future, nanoscale optical on-chip communication [32-34]. Light

*mantu@vt.edu; Tel: 540-231-6663; Fax: 540-231-3362; adsel.ece.vt.edu

Quantum Sensing and Nano Electronics and Photonics XIII, edited by Manijeh Razeghi, Gail J. Brown, Jay S. Lewis, Proc. of SPIE Vol. 9755, 97550Y · © 2016 SPIE
CCC code: 0277-786X/16/$18 · doi: 10.1117/12.2218364

sources with directly-grown active materials are needed for the large-scale integration of highly-integrated photonic devices for optical interconnects in future high-capacity datacenters and high-performance computing applications. Furthermore, optical interconnects compatible with Si process technology are needed to provide for ever-increasing future bandwidth needs [35]. Moreover, the electrical-to-optical interconnect transition for chip-to-chip communication is expected to be a gradual process depending upon specific application requirements and cost-performance trade-offs with current copper-based interconnect technologies [36]. This paper presents a novel, monolithic heterogeneous integration scheme for group-IV-based lasers with tunable wavelengths utilizing a combination of all-epitaxial strain-engineered biaxial tensile-strained Ge (ε-Ge) and III-V compound semiconductors integrated on Si substrates. Our hybrid ε-Ge/III-V materials integration approach on Si offers greater design flexibility, diverse material choices, and a path towards the monolithic integration of electronic and photonic devices on the same Si platform. The tunable ε-Ge heterogeneously grown on GaAs and Si substrates *via* graded $In_xGa_{1-x}As$ and $In_xAl_{1-x}As$ buffer architectures were grown

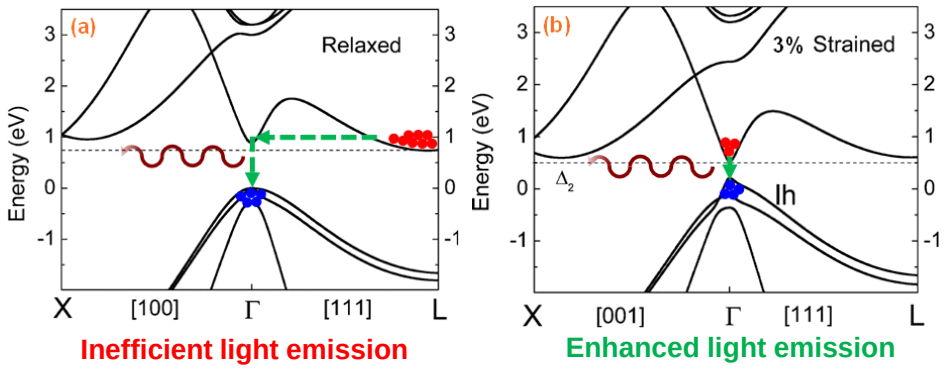

Figure 1: (a) Unstrained Ge phonon-assisted indirect recombination and (b) strain-engineered Ge exhibiting direct recombination. [31]

by solid source molecular beam epitaxy (MBE). The detailed structural, morphological, energy band alignment, and optical properties of these tunable ε-Ge thin films offer a modular approach towards designing group-IV lasers heterogeneously integrated on Si displaying tunable wavelengths ranging from 1.55 μm to 2.1 μm.

2. EXPERIMENTAL PROCEDURE

2.1 Materials Synthesis

Unintentionally doped ε-Ge epilayers with thicknesses of 15 nm - 40 nm were grown on semi-insulating (100)/2° offcut GaAs and n-type (100)/4-6° offcut Si substrates using an *in-situ* growth process utilizing separate solid-source MBE growth chambers for the Ge and III-V materials, connected *via* an ultra-high vacuum transfer chamber. The combined effects of substrate offcut and the controlled nucleation of GaAs (*i.e.*, low growth temperature and low growth rate with an As_2 pre-layer during nucleation) suppressed the formation of anti-phase domains due to polar-on-nonpolar growth (*i.e.*, GaAs on Si). The GaAs nucleation layer was followed by standard GaAs epitaxy at 650°C using a 0.5 μm/hr growth rate, thereby creating a "virtual" metamorphic template on Si for subsequent epilayer growth. Subsequently, $In_xGa_{1-x}As$ strain templates with pre-defined indium (In) alloy compositions were grown on linearly graded $In_xGa_{1-x}As$, thereby utilizing the $In_xGa_{1-x}As$/GaAs composite metamorphic buffer to mitigate defects and dislocations due to the lattice and thermal mismatch between Ge and Si. Several $In_xGa_{1-x}As$ buffers with different terminating In compositions (0%–29% In for 0%–1.95% in-plane biaxial tensile strain) were grown using the III-V MBE chamber prior to Ge strained-layer epitaxy. Similarly, an alternative large bandgap buffer architecture that can be used to grow ε-Ge is $In_xAl_{1-x}As$. This mixed cation-graded buffer can provide the large band offsets needed for carrier and optical confinement in tunable ε-Ge-based lasers. During the substrate oxide desorption and throughout each layer growth, reflection high energy electron diffraction (RHEED) was used to monitor the surface reconstruction as well as for growth-induced defects (if any). After each $In_xGa_{1-x}As$/GaAs template was grown on either GaAs or Si, the sample was transferred *via* an ultra-high vacuum transfer chamber to the Ge MBE chamber for subsequent ε-Ge growth. In all cases, a growth temperature of 400°C and growth rate of ~0.1Å/s were used for strained-layer Ge epitaxy. The growth temperatures in this work refer to the thermocouple temperature maintained during epitaxy. The ε-Ge on GaAs and Si samples were characterized by high-resolution X-ray diffraction, atomic force microscopy, cross-sectional transmission electron

microscopy (TEM) and low temperature photoluminescence measurement. After structural, morphological and optical characterization, selected samples were transferred to the III-V MBE chamber for the upper $In_xGa_{1-x}As$ layer growth. Prior to the $In_xGa_{1-x}As$ cap layer growth, samples were held at 400°C for ~30 min to thermally desorb residual Ge surface oxides formed during *ex-situ* materials characterization. RHEED was used to monitor the surface reconstruction of the ε-Ge layer during the oxide desorption as well as the upper $In_xGa_{1-x}As$ layer growth. RHEED characterization exhibited (2x2) surface reconstruction for the ε-Ge layer. Since the native oxides on ε-Ge are unstable, a lower thermal budget was selected to prevent strain relaxation and atomic species interdiffusion at the ε-Ge/$In_xGa_{1-x}As$ heterointerface. Moreover, a higher temperature would increase the surface roughening during the upper InGaAs layer growth. The thorough desorption of native oxides from the ε-Ge epilayer is crucial for achieving an atomically abrupt, oxide-free heterointerface, thereby reducing the likelihood of generating electrically or optically active interfacial defect states.

2.2 Materials Characterization

To study the surface reconstruction of the GaAs or Si substrates as well as the ε-Ge on InGaAs, RHEED patterns were recorded at different stages during growth. The surface morphology of each structure was determined by Nomarski optical microscopy and atomic force microscopy. To determine the crystalline quality and relaxation state of the ε-Ge layers grown on GaAs and Si, high-resolution triple axis X-ray rocking curves and reciprocal space maps were recorded from each sample using a Panalytical X-pert Pro system equipped with both PIXel and proportional detectors with a monochromatic CuKα (λ = 1.540598 Å) X-ray source. High-resolution cross-sectional TEM was used to characterize the long-range structural quality and abruptness of each ε-Ge/$In_xGa_{1-x}As$ heterointerface. The imaging was performed using a JEOL 2100 transmission electron microscope. For this purpose, electron transparent foils of thin film cross-sections of each sample structure were prepared by standard polishing techniques, *i.e*. mechanical grinding, dimpling and low-temperature Ar^+ ion beam milling. The bandgap as a function of strain within each ε-Ge epilayer was characterized *via* micro-photoluminescence (μ-PL) spectroscopy using an 800 nm laser source and a thermoelectric cooled InGaAs detector for optical pumping and detection, respectively. The band alignment at each ε-Ge/$In_xGa_{1-x}As$ heterointerface was investigated using a PHI Quantera SXM XPS system with a monochromatic Al-Kα (E = 1486.7 eV) X-ray source. Additionally, we have recently demonstrated the band alignments of tunable ε-Ge/$In_xGa_{1-x}As$ systems [37-39].

3. RESULTS

3.1 Reflection High Energy Electron Diffraction Studies

To study the surface reconstruction of the GaAs or Si substrates, the ε-Ge on $In_xGa_{1-x}As$, and the $In_xGa_{1-x}As$ layer on ε-Ge, RHEED patterns were recorded at different stages of growth. Figure 2 shows RHEED patterns along the [100] azimuth for the growth sequence of Ge/$In_{0.16}Ga_{0.84}As$/$In_xGa_{1-x}As$/(100)6°GaAs: (a) the (100) GaAs substrate shows a (2x4) pattern and (b) the 0.75% ε-Ge layer shows (2x2) surface reconstruction. RHEED patterns from the surface of Ge were also recorded after transferring the structure from the Ge MBE to the III-V MBE chamber through the ultra-high vacuum transfer chamber. The GaAs surface exhibited (2x4) surface reconstruction, as expected, and the streaky (2x2) pattern of the ε-Ge layer (0%–1.95%) on GaAs or Si substrates suggests a smooth surface morphology. Hence, the surface reconstruction of Ge as a function of In alloy composition in the ternary $In_xGa_{1-x}As$ buffer (*i.e*., with different Ge tensile strain states) is vital in providing information related to the uniformity of the ε-Ge surface morphology.

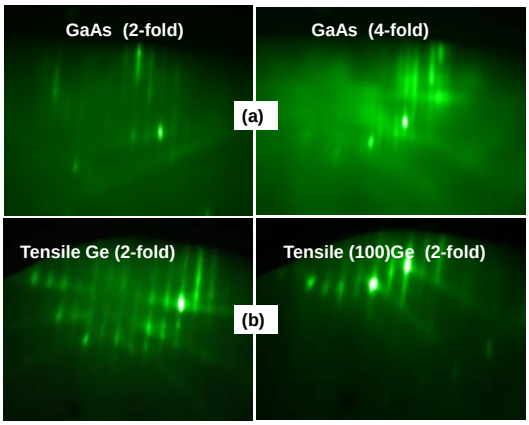

Figure 2: RHEED patterns from the surface of (a) GaAs substrate and (b) ε-Ge layer along the azimuth of [100].

3.2 Surface Morphology Characterization

It is important to characterize the surface morphology (*e.g.*, roughness, surface features) for metamorphic structures due to the expected crosshatch resulting from ideal strain relaxation with minimum concentrations of threading dislocations, which is an important figure of merit. Nomarski optical micrographs from the surface of ε-Ge grown on GaAs using graded $In_xGa_{1-x}As$ and $In_xAl_{1-x}As$ buffers and on Si using a composite GaAs and graded $In_xGa_{1-x}As$ buffer are shown in Figure 3. One can see a well-developed, extremely uniform two-dimensional crosshatch pattern for the ε-Ge grown on GaAs using either graded $In_xGa_{1-x}As$ or $In_xAl_{1-x}As$, as expected for an ideal graded buffer. However, the ε-Ge on $In_xAl_{1-x}As$ morphology also reveals a grainy texture dispersed across the surface upon closer observation. The grainy texture is more prominent on the ε-Ge grown on Si due to the higher lattice mismatch between the ε-Ge and the Si substrate, indicating that more dislocations are present inside the active layer as comparted to the sample grown on GaAs. The AFM images in Figure 3 provide a clearer and quantifiable picture of the differences. The root mean square (rms) surface roughness for the ε-Ge grown using relaxed $In_xGa_{1-x}As$ is 3.35 nm as opposed to 7.39 nm for the ε-Ge grown on Si, measured over an area of 20×20 μm^2, which is consistent with the Nomarksi optical microscopy data.

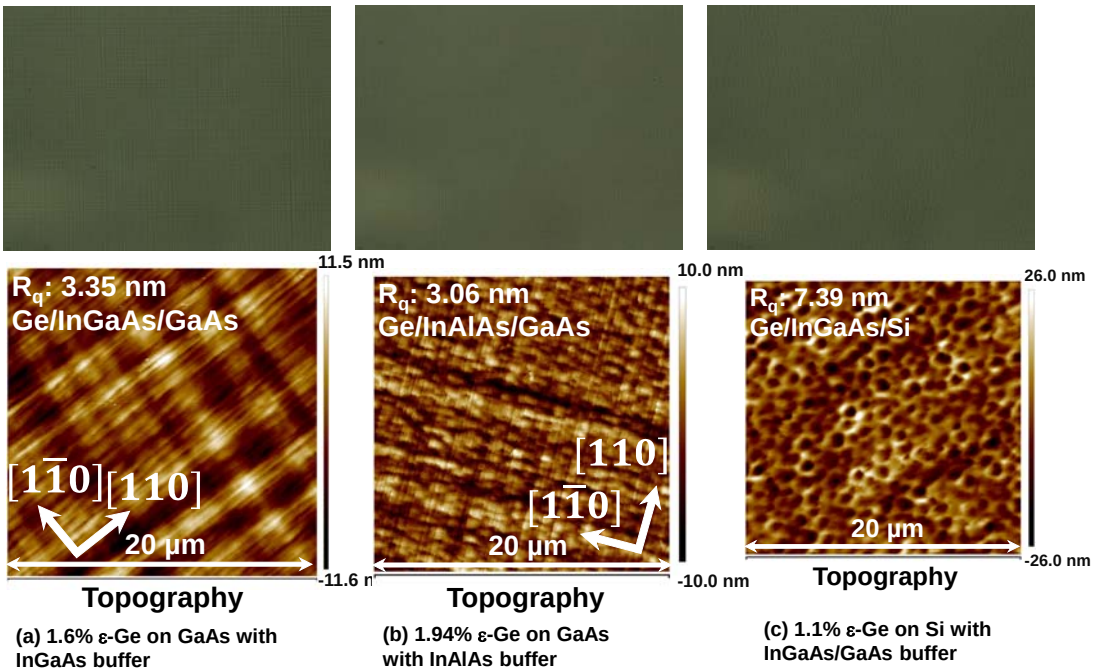

(a) 1.6% ε-Ge on GaAs with InGaAs buffer

(b) 1.94% ε-Ge on GaAs with InAlAs buffer

(c) 1.1% ε-Ge on Si with InGaAs/GaAs buffer

Figure 3: Nomarski and atomic microscopy images of (a) 1.6% ε-Ge, (b) 1.95% ε-Ge, and (c) 1.11% ε-Ge on GaAs and Si substrates using graded $In_xGa_{1-x}As$ and $In_xAl_{1-x}As$ buffers on GaAs and a composite buffer ($In_xGa_{1-x}As$/GaAs) on Si, respectively.

3.3 Strain Relaxation Properties of Varying ε-Ge Grown on GaAs

To determine the structural quality and strain state of the Ge epilayers as a function of strain from 0.75% to 1.95%, X-ray rocking curves and reciprocal space maps (RSMs) of symmetric (004) and asymmetric (115) scattering geometries were recorded from each of the ε-Ge heterostructures. Figure 4 shows (a) rocking curves for 0.75% ε-Ge, 1.6% ε-Ge, 1.95% ε-Ge, as well as (004) and (115) RSMs for (b) 1.6% ε-Ge, and (c) 1.95% ε-Ge, respectively, grown on GaAs substrates. One can find from this figure that the Ge is tensile strained with respect to each constant composition $In_xGa_{1-x}As$ strain template. Compositionally graded $In_xGa_{1-x}As$ metamorphic buffers with different terminating In compositions were selected to produce tunable tensile-strained Ge epilayers, as shown in Figure 4 (a), as well as to mitigate defects and dislocations due to the lattice and thermal mismatch between the ε-Ge and the GaAs substrate. The GaAs or $In_xGa_{1-x}As$ layer thickness on top of the ε-Ge was carefully selected such that the upper lattice matched top-GaAs/ε-Ge or top-$In_xGa_{1-x}As$/ε-Ge is fully strained, as shown by the dotted strain line in each figure. In these structures, the combined thickness of upper $In_xGa_{1-x}As$ (or GaAs) and ε-Ge layer was selected carefully to prevent the relaxation of the ε-Ge. One can find from X-ray analysis that the Ge layer is indeed tensile strained since the reciprocal lattice point (RLP) of Ge is located above the GaAs RLP. Moreover, the RLPs of the GaAs substrate, the uppermost composition of $In_xGa_{1-x}As$ and

ε-Ge are along the same vertical line, indicating a minimal or near absence of lattice tilt with respect to the GaAs substrate. In all cases, the overlying GaAs or $In_xGa_{1-x}As$ growth on the ε-Ge epilayer is expected to form an optical cavity, necessary for carrier and optical confinement in tunable group-IV-based lasers.

3.4 Strain Relaxation Properties of Varying ε-Ge Heterogeneously Grown on Si

The ε-Ge/$In_xGa_{1-x}As$ heterostructures with tunable Ge strain levels were heterogeneously integrated on Si using composite metamorphic III-V buffers. The composite buffer architecture consisted of GaAs and linearly graded $In_xGa_{1-x}As$ with varying terminating In alloy compositions, resulting in Ge tensile strain states from 0% to 1.11% [39]. Moreover, the composite metamorphic GaAs and graded $In_xGa_{1-x}As$ buffer allowed for the mitigation of lattice-mismatch-induced defects between the active layer and the Si substrate. The ultimate goal was to achieve symmetrical strain relaxation of these buffers. If this property is maintained after the growth of the Ge epilayer, which is lattice-matched to the in-plane lattice constant of the graded buffer, then the terminal layer of the metamorphic buffer can be considered as a "virtual" substrate on Si. Figure 5 shows (a) the X-ray rocking curves for the ε-Ge structures with 0.82% and 1.11% tensile strain and (b), the (115) asymmetric reciprocal space map from 1.11% ε-Ge/$In_{0.17}Ga_{0.83}As$. One can find from Figure 5 (b) that the ε-Ge RLP lies above the GaAs RLP, confirming the tensile nature of the strain held by the Ge epilayer. Furthermore, the RLPs of the ε-Ge and the $In_xGa_{1-x}As$ virtual substrate lie along the same vertical line in reciprocal space, further confirming the pseudomorphic nature of the ε-Ge. Additionally, the ε-Ge and GaAs RLPs are partially superimposed due to the moderate strain levels in the Ge and the broadening of the GaAs virtual substrate RLP as a result of lattice mismatch with the Si substrate. However, the RLPs of Si, GaAs, and graded $In_xGaA_{1-x}s$ are clearly visible. Thus, the successful demonstration of ε-Ge on varying In alloy composition $In_xGa_{1-x}As$/GaAs metamorphic buffers on Si is an important step towards tuning the bandgap of Ge through band structure engineering as well as tailoring the band alignment at the ε-Ge/$In_xGa_{1-x}As$ heterointerface for enhanced carrier and optical confinement.

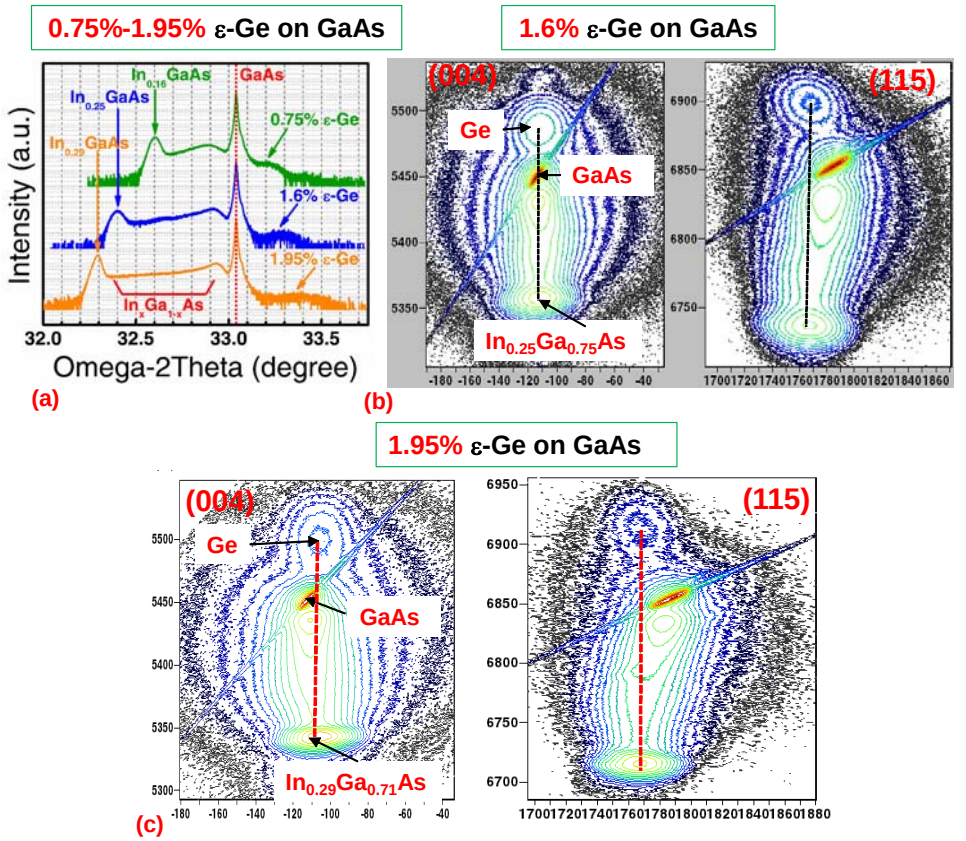

Figure 4: X-ray (a) rocking curve, (004) and (115) RSMs for (b) 1.6% ε-Ge and (c) 1.95% ε-Ge grown on GaAs substrates, respectively. The different tensile Ge strain states were produced by growing different In alloy composition $In_xGa_{1-x}As$ strain templates. The Ge is fully strained, as indicated by the strain line (shown in red) as well as the peak location of the e-Ge with respect to the GaAs substrate.

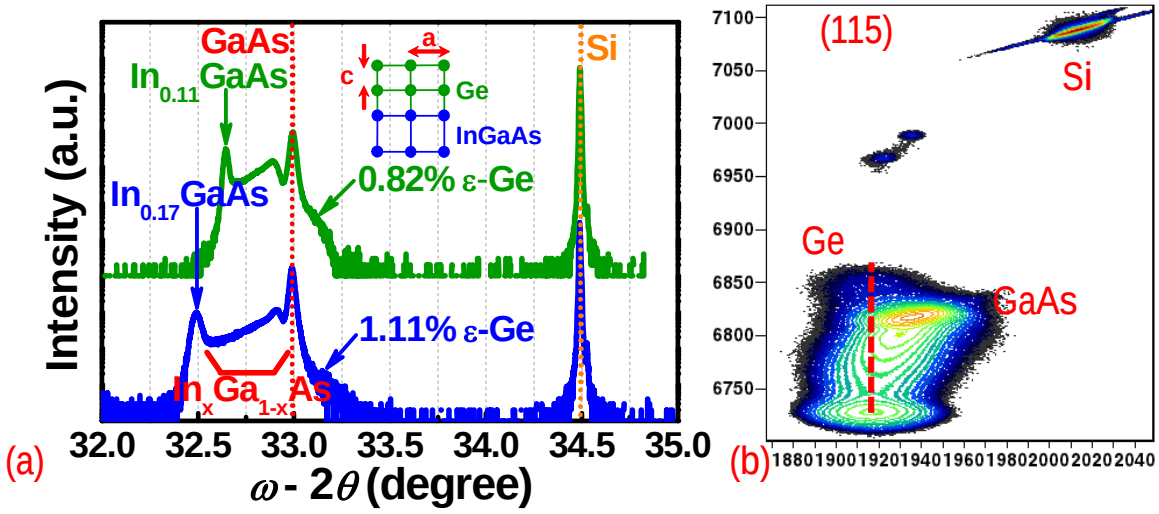

Figure 5: X-ray (a) rocking curve and (115) RSM for (b) 1.11% ε-Ge grown on Si substrates [39]. The Ge is fully strained as indicated by the strained line in x-ray.

3.5 $In_xAl_{1-x}As$ Buffer Architectures on GaAs or Si for Strain-Engineered Ge

As discussed above, the $In_xAl_{1-x}As$ buffer architecture can also be used for strain-engineering the band structure of Ge. Figure 6 shows the asymmetric (115) RSM of the 1.95% ε-Ge grown on GaAs using a linearly graded $In_xAl_{1-x}As$ metamorphic buffer. In this figure, one can find that the RLPs of Ge, GaAs, and the $In_{0.27}Al_{0.73}As$ virtual substrate are clearly visible. In such buffer layers (*e.g.*, $In_xGa_{1-x}As$ or $In_xAl_{1-x}As$), the ε-Ge will be internally lattice matched such that the active lasing media (ε-Ge) is free from dislocations generated due to lattice mismatch at the heterointerface with the cladding layers. Moreover, the ability to select between several buffer architectures offers a highly customizable substrate platform for optical devices that leverage the band structure engineering of Ge. Therefore, we have successfully developed metamorphic buffer strategies, as evident by the fully relaxed nature and low surface roughness of III-V buffers on GaAs or Si, that offer greater design flexibility for the realization of tunable group-IV-based lasers heterogeneously integrated on Si.

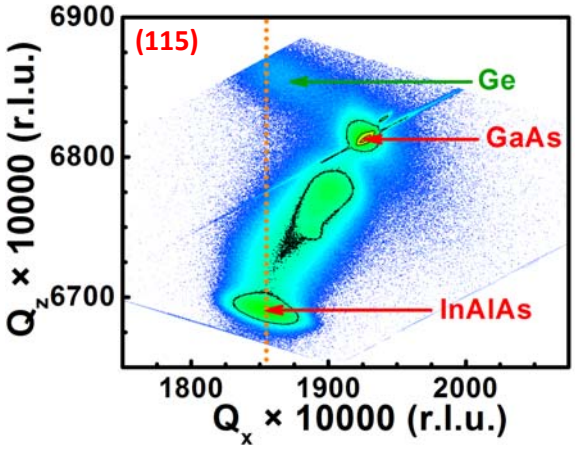

Figure 6: X-ray (115) RSM of ~1.95% ε-Ge grown on $In_{0.27}Al_{0.73}As/In_xAl_{1-x}As$/GaAs substrate. The Ge is almost fully strained, as indicated by the vertical strained line.

3.6 Cross-sectional TEM Analysis of ε-Ge on GaAs and Si

Figure 7 shows high-resolution cross-sectional TEM micrographs of ε-Ge/$In_{0.16}Ga_{0.84}As$ (0.75% ε-Ge) on GaAs [37] and ε-Ge/$In_{0.17}Ga_{0.83}As$ (1.11% ε-Ge) on Si [39], respectively. One can find that lattice-mismatch-induced dislocations are confined within the graded $In_xGa_{1-x}As$ buffer layer and that the ε-Ge/$In_xGa_{1-x}As$ active regions are free from defects (at this scale). The high resolution lattice indexing shows the lattice line extending from the ε-Ge layer to $In_{0.16}Ga_{0.84}As$ ($In_{0.17}Ga_{0.83}As$), signifying that the Ge in-plane lattice constant is internally matched with the lattice constant of the $In_{0.16}Ga_{0.84}As$ ($In_{0.17}Ga_{0.83}As$) layer, which is also supported by the X-ray analysis above. Moreover, Fast-Fourier Transform (FFT) patterns from these samples further demonstrate the matching of the in-plane lattice constant of ε-Ge with respect to the underlying $In_xGa_{1-x}As$ strain template. Thus, the cross-sectional TEM micrographs validate the pseudomorphic nature of the ε-Ge epilayer, where the Ge lattice constant matches the in-plane lattice constant of the $In_xGa_{1-x}As$ virtual substrate. Therefore, one can feasibly vary the In composition in the graded buffer layer such that the overlying Ge is tensile strained, exhibiting direct-gap recombination and ultimately allowing for the realization of tunable light sources emitting in the 1.55 μm to 2.1 μm wavelength range on Si.

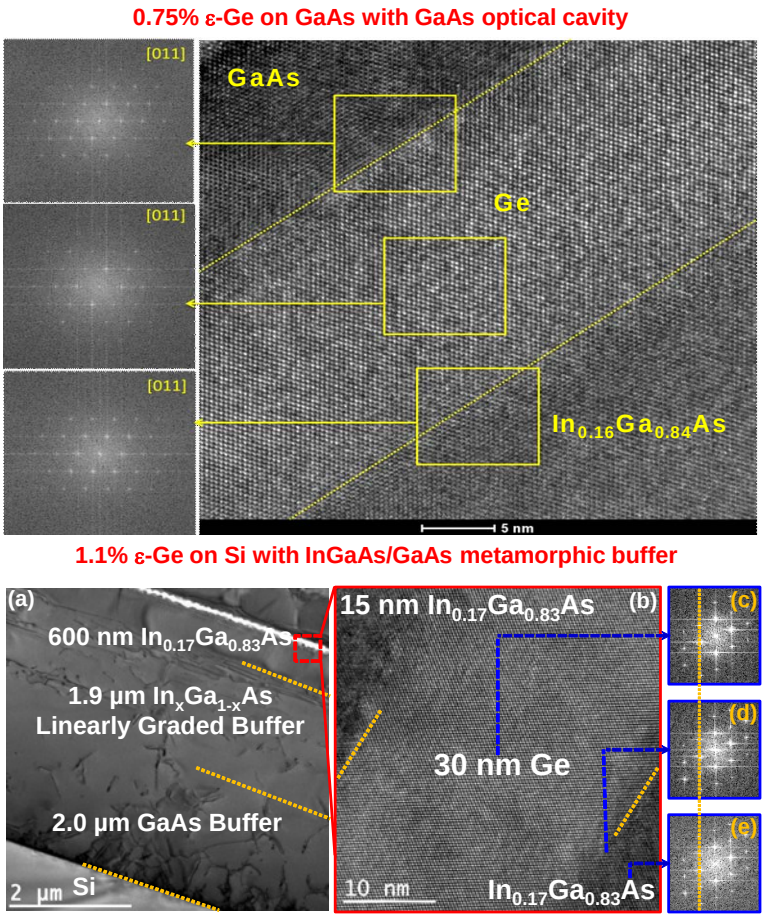

Fig. 7: High-resolution cross-sectional TEM micrograph of 0.75% strained GaAs/Ge/$In_{0.16}Ga_{0.86}As$ [37] structure on GaAs and 1.11% ε-Ge on Si [39]. The lattice line indexing and the FFT patterns demonstrate the lattice-matching of the ε-Ge with the in-plane lattice constant of the underlying $In_xGa_{1-x}As$ layer.

3.7 Laser Cavity, Optical Measurements, and Schematic of Mode-Locked ε-Ge Laser

One of the most critical design parameters for future ε-Ge-based lasers is the proper selection of an optical cladding material. In this work, we have selected a III-V (GaAs or $In_xGa_{1-x}As$), lattice-matched cladding layer that will enhance

carrier and optical confinement in the ε-Ge waveguide. Moreover, measures must be taken to select an upper cladding layer thickness in order to (i) prevent the relaxation of the ε-Ge QW, (ii) achieve superior optical confinement, and (iii) achieve low-loss guided lasing modes in the ε-Ge QW. The thickness and composition are also important such that the refractive indices of the various layers are suitable for strong optical confinement. In this work, low-temperature micro-photoluminescence (μ-PL) measurements were performed at 7.5K utilizing an incident power density of 860 kW/cm^2 and excitation wavelength of 800 nm. Figure 8 (a) shows the PL spectra obtained from 0% to 1.6% ε-Ge with and without capping layers. The PL spectra have been shifted vertically for clarity. One can see from Figure 8 (a) that the main peak position is red-shifted towards lower photon energies (higher wavelengths) due to the increase in tensile strain and corresponding reduction in ε-Ge bandgaps. Figure 8 (b) compares the experimentally observed bandgaps (symbols) and strain determined from XRD analysis, respectively, with the predicted dependence of the low-temperature Ge bandgap on increasing strain (solid lines) calculated using a 30×30 ***k·p*** formalism. Additionally, the effect of decreasing ε-Ge epilayer thickness (t_{Ge}) on the ε-Ge bandgap due to energy level quantization is shown via the dashed (t_{Ge} = 40 nm) and dotted (t_{Ge} = 30 nm) lines. There is an excellent agreement with the theoretical bandgap-strain relation shown in Figure 8 (b). Figure 9 shows the schematic of a ε-Ge QW-based laser on Si. These lasers will be tunable in wavelength as a function of band structure engineering through strain-engineering and QW geometry. Furthermore, the demonstration of tunable wavelength ε-Ge epitaxial layers heterogeneously integrated onto Si is a key first step towards the monolithic integration of Ge-based photonic devices and optically active layers with state-of-the-art CMOS technology as well as the development of energy-efficient light sources for future on-chip optical interconnects.

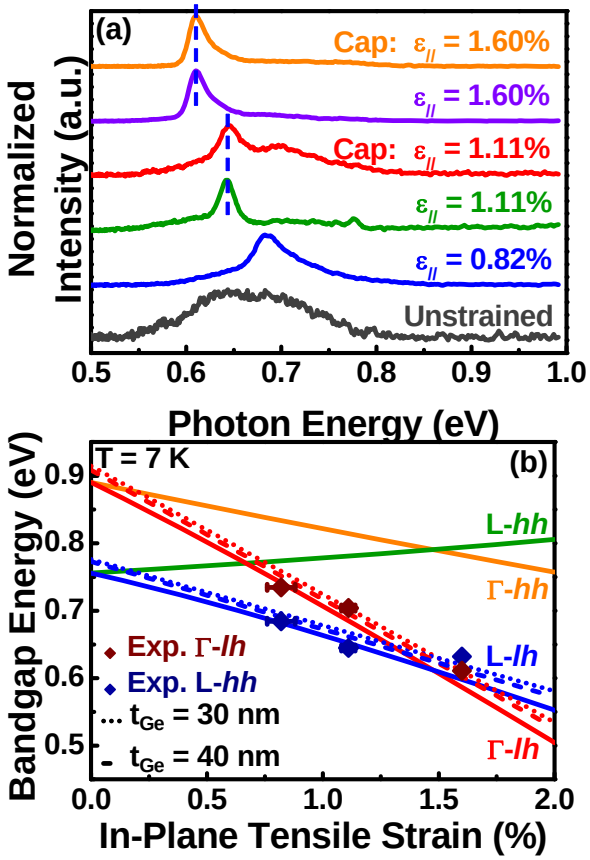

Figure 8: (a) Red-shift (plotted in photon energy) due to strain in the ε-Ge epilayers as measured by μ-PL at 7.5 K. (b) μ-PL determined bandgaps of 0.82%–1.6% ε-Ge in comparison to the theoretical bandgap-strain dependence for Ge calculated using a 30×30 ***k·p*** model taking into quantization-induced bandgap enhancement at decreased ε-Ge layer thicknesses. Good agreement is found between the measured (symbols) and predicted (lines) bandgaps as a function of increasing tensile strain.

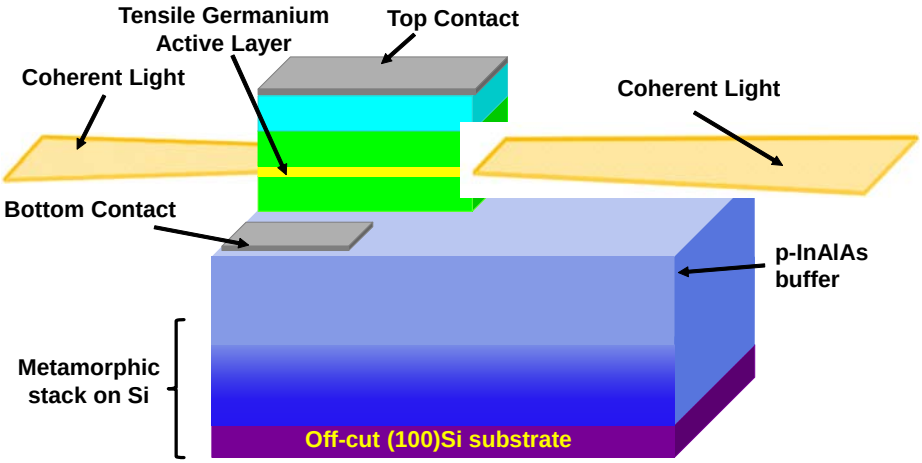

Figure 9: Schematic of the ε-Ge mode-locked QW laser on Si.

4. CONCLUSION

In this work, we have demonstrated tunable tensile-strained Ge on GaAs and heterogeneously integrated on Si using composite GaAs and linearly graded $In_xGa_{1-x}As$ ($In_xAl_{1-x}As$) buffers grown by solid source molecular beam epitaxy for strain-engineered group-IV-based lasers on Si. High-resolution X-ray diffraction provided the strain state of each ε-Ge layer as well as the micro structural quality of the Ge thin films and buffer architectures. Sharp heterointerfaces between each ε-Ge epilayer and the respective $In_xGa_{1-x}As$ virtual substrate were demonstrated by high-resolution cross-sectional transmission electron microscopy. Low-temperature micro-photoluminescence measurements demonstrated direct band gap Ge as a function of strain, which was further corroborated theoretically using a 30×30 ***k·p*** formalism. The successful demonstration of a III-V/ε-Ge/III-V quantum well/optical cavity configuration and an all-epitaxial heterogeneous integration scheme on Si pave the way for the realization of novel group-IV-based strain-engineered tunable light sources on Si.

Acknowledgements. M. C. acknowledges financial support from the NSF under grant numbers ECCS-1348653 and ECCS-1507950. Authors acknowledge the Institute for Critical Technology and Applied Science-NCFL and Virginia Tech Nanofabrication facilities for materials characterization. Authors also acknowledge Aheli Ghosh for helping to generate the schematic of the mode-locked laser.

REFERENCES

[1] International Technology Roadmap for Semiconductors; (2013). http://www.itrs.net/home.html

[2] Chau, R., Doyle, B., Datta, S., Kavalieros, J. and Zhang, K., "Integrated Nanoelectronics for the Future", Nat. Mat. 6, 810-812 (2007).

[3] Heyns, M., Alian, A., Brammertz, G., Caymax, M., Chang, Y. C., Chu, L. K., De Jaeger, B., Eneman, G., Gencarelli, F., Groeseneken, G., Hellings, G., Hikavyy, A., Hoffmann, T. Y., Houssa, M., Huyghebaert, D., Leonelli, D., Lin, D., Loo, R., Magnus, W., Merckling, C., Meuris, M., Mitard, J., Nyns, L., Orzali, T., Rooyackers, R., Sioncke, S., Soree, B., Sun, X., Vandooren, A., Verhulst, A. S., Vincent, B., Waldron, N., Wang, G., Wang, W. E. and Witters, L., "Advancing CMOS Beyond the Si Roadmap with Ge and III/V Devices", In IEEE Int. Electron Devices Meet. (IEDM), Washington, DC, Dec. 5-7, IEEE: New York, 2011; DOI: 10.1109/IEDM.2011.6131543 (2011).

[4] Chau, R., Datta, S. and Majumdar, A., "Opportunities and Challenges of III-V Nanoelectronics for Future High-Speed, Low-Power Logic Applications", In IEEE Compound Semiconductor Integrated Circuit Symposium

(CSICS) Tech. Dig., Palm Springs, CA, Oct. 30-Nov. 2, 2005; IEEE: New York, 2005; DOI: 10.1109/CSICS.2005.1531740 (2005).

[5] Zhang, Q., Fang, T., Xing, H., Seabaugh, A. and Jena, D., "Graphene Nanoribbon Tunnel Transistors", IEEE Electron Device Lett. 29, 1344-1346 (2008).

[6] Kavalieros, J., Doyle, B., Datta, S., Dewey, G., Doczy, M., Jin, B., Lionberger, D., Metz, M., Rachmady, W., Radosavljevic, M., Shah, U., Zelick, N. and Chau, R., "Tri-Gate Transistor Architecture with High-k Gate Dielectrics, Metal Gates and Strain Engineering", In VLSI Technology, 2006. Digest of Technical Papers. 2006 International Symposium on VLSI Technology, Systems, and Applications, Honolulu, HI, June 13-15, 2006; IEEE: New York, 2006; DOI: 10.1109/VLSIT.2006.1705211 (2006).

[7] Seabaugh A. C. and Zhang, Q., "Low-Voltage Tunnel Transistors for Beyond CMOS Logic", Proc. IEEE 98, 2095-2110 (2010).

[8] Ionescu A. M. and Riel, H., "Tunnel Field-Effect Transistors as Energy-efficient Electronic Switches", Nature 479, 329-337 (2011).

[9] Auth, C. P. and Plummer, J. D., "Scaling Theory for Cylindrical, Fully-Depleted, Surrounding-Gate MOSFET's", IEEE Electron Device Lett. 18, 74-76 (1997)

[10] Datta, S., Dewey, G., Fastenau, J. M., Hudait, M. K., Loubychev, D., Liu, W. K., Radosavljevic, M., Rachmady W. and Chau, R., "Ultrahigh-Speed 0.5 V Supply Voltage $In_{0.7}Ga_{0.3}As$ Quantum-Well Transistors on Silicon Substrate", IEEE Electron Device Lett. 28, 685-687 (2007).

[11] Yang, J. J., Pickett, M. D., Li, X., Ohlberg, D. A., Stewart D. R. and Williams, R. S., "Memristive Switching Mechanism for Metal/Oxide/Metal Nanodevices", Nat. Nanotechol. 3, 429-433 (2008).

[12] Miller, D. A. B., "Device Requirements for Optical Interconnects to Silicon Chips", Proc. IEEE 97, 1166-1185 (2009).

[13] Miller, D. A. B., "Physical Reasons for Optical Interconnection", Int. J. Optoelectronics 11, 155-168 (1997).

[14] Liang D. and Bowers, J. E., "Recent Progress in Lasers on Silicon", Nat. Photonics 4, 511-517 (2010).

[15] Koshida N. and Koyama, H., "Visible Electroluminescence from Porous Silicon", Appl. Phys. Lett. 60, 347-349 (1992).

[16] Pavesi, L., Dal Negro, L., Mazzoleni, C., Franzo G. and Priolo, F., "Optical Gain in Silicon Nanocrystals", Nature 408, 440-444 (2000).

[17] Saito, S., Hisamoto. D., Shimizu, H., Hamamura, H., Tsuchiya, R., Matsui, Y., Mine, T., Arai, T., Sugii, T., Torii, K., Kimura S. and Onai, T., "Silicon Light-emitting Transistor for On-chip Optical Interconnection", Appl. Phys. Lett. 89, 163504 (2006).

[18] Kenyon, A. J., Trwoga, P. F., Federighi, M. and Pitt, C. W., "Optical Properties of PECVD Erbium-doped Silicon-rich Silica: Evidence for Energy Transfer between Silicon Microclusters and Erbium Ions", J. Phys. Condens. Matter 6, L319-L324 (1994).

[19] He, G. and Atwater, H. A., "Interband Transitions in Sn_xGe_{1-x} Alloys", Phys. Rev. Lett. 79, 1937-1940. (1997).

[20] Rong, H., Liu, A., Jones, R., Cohen, O., Hak, D., Nicolaescu, R., Fang, A. and Paniccia, M., "An all-Silicon Raman Laser", Nature 433, 292-294 (2005).

[21] Groenert, M. E., Leitz, C. W., Pitera, A. J., Yang, V., Lee, H., Ram, R. J. and Fitzgerald, E. A., "Monolithic Integration of Room-temperature GaAs/AlGaAs Lasers on Si Substrates via Relaxed Graded GeSi Buffer Layers", J. Appl. Phys. 93, 362-367 (2003)

[22] Fang, A. W., Park, H., Cohen, O., Jones, R., Paniccia, M. J. and Bowers, J. E., "Electrically Pumped Hybrid AlGaInAs-Silicon Evanescent Laser", Opt. Express 14, 9203-9210 (2006)

[23] Saito, S., Takahama, T., Tani, K., Takahashi, M., Mine, T., Suwa, Y. and Hisamoto, D., "Stimulated Emission of Near-infrared Radiation in Silicon fin Light-emitting Diode", Appl. Phys. Lett. 98, 261104 (2011).

[24] Yang, J., Bhattacharya, P. and Wu, Z., "Monolithic Integration of InGaAs-GaAs Quantum-Dot Laser and Quantum-Well Electroabsorption Modulator on Silicon", IEEE Photon. Tech. Lett. 19, 747-749 (2007).

[25] Jongthammanurak, S., Liu, J., Wada, K., Cannon, D. D., Danielson, D. T., Pan, D., Kimerling, L. C.and Michel, J., "Large Electro-Optic Effect in Tensile Strained Ge-on-Si Films", Appl. Phys. Lett. 89, 161115-1—161115-3 (2006)

[26] Kuo, Y. H., Lee, Y. K., Ge, Y., Ren, S., Roth, J. E., Kamins, T. I., Miller, D. A. B. and Harris, J. S., "Strong Quantum-Confined Stark Effect in Germanium Quantum-Well Structures on Silicon", Nature 437, 1334-1336 (2005).

[27] Ahn, D., Hong, C. Y., Liu, J., Giziewicz, W., Beals, M., Kimerling, L. C., Michel, J., Chen, J. and Kartner, F. X., "High Performance, Waveguide Integrated Ge Photodetectors", Opt. Express 15, 3916-3921 (2007).

[28] Vivien, L., Rouviere, M., Fedeli, J. M., Marris-Morini, D., Damlencourt, J. F., Mangeney, J., Crozat, P., El Melhaoui, L., Cassan, E., Le Roux, X., Pascal, D. and Laval, S., "High Speed and High Responsivity Germanium Photodetector Integrated in a Silicon-On-Insulator Microwaveguide", Opt. Express 15, 9843-9848 (2007).

[29] Roth, J. E., Fidaner, O., Schaevitz, R. K., Kuo, Y. H., Kamins, T. I., Harris, J. S. and Miller, D. A. B., "Optical Modulator on Silicon Employing Germanium Quantum Wells", Opt. Express 15, 5851-5859 (2007).

[30] Feng, N. N., Feng, D., Liao, S., Wang, X., Dong, P., Liang, H., Kung, C. C., Qian, W., Fong, J., Shafiiha, R., Luo, Y., Cunningham, J., Krishnamoorthy A. V. and Asghari, M., "30GHz Ge Electro-Absorption Modulator Integrated with 3μm Silicon-on-Insulator Waveguide", Opt. Express 19, 7062-7067 (2011).

[31] El Kurdi, M., Fishman, G., Sauvage, S. and Boucaud, P., "Band Structure and Optical Gain of Tensile-Strained Germanium Based on a 30 Band k•p Formalism", J. Appl. Phys. 107, 013710-1-013710-7 (2010).

[32] Liu, J., Sun, X., Camacho-Aguilera, R., Kimerling L. C. and Michel, J., "Ge-on-Si Laser Operating at Room Temperature", Opt. Lett. 35, 679-681 (2010).

[33] Camacho-Aguilera, R. E., Cai, Y., Patel, N., Bessette, J. T., Romagnoli, M., Kimerling, L. C. and Michel, J., "An Electrically Pumped Germanium Laser", Opt. Express 20, 11316-11320 (2012).

[34] Cho, S., Park, B.,G., Yang, C., Cheung, S., Yoon, E., Kamins, T. I., Yoo S. J. B. and Harris, J. S., "Room-Temperature Electroluminescence from Germanium in an Al0.3Ga0.7As/Ge Heterojunction Light-Emitting Diode by Γ-Valley Transport",Opt. Express 20, 14921-14927 (2012).

[35] Assefa, S., Xia F. and Vlasov, Y. A., "Reinventing Germanium Avalanche Photodetector for Nanophotonic On-Chip Optical Interconnects", Nature 464, 80-84 (2010).

[36] Mi, Z., Yang, J., Bhattacharya, P., Qin, G. and Ma, Z., "High-Performance Quantum Dot Lasers and Integrated Optoelectronics on Si". Proc. IEEE 97, 1239-1249 (2009).

[37] Zhu, Y., Maurya, D., Priya, S. and Hudait, M. K., "Tensile-Strained Nanoscale Ge/$In_{0.16}Ga_{0.84}As$ Heterostructure for Tunnel Field-Effect Transistor", ACS Appl. Mater. Interfaces 6, 4947-4953 (2014).

[38] Clavel, M., Goley, P. S., Jain, N., Zhu, Y. and Hudait, M. K., "Strain Engineered Biaxial Tensile Epitaxial Germanium for High-Performance Ge/InGaAs Tunnel Field-Effect Transistors", IEEE J. Elec. Dev. Soc. 3, 184-193 (2015).

[39] Clavel, M., Saladukha, D., Goley, P., Ochalski, T. J., Murphy-Armando, F., Bodnar, R. J. and Hudait, M. K., "Heterogeneously-Grown Tunable Tensile Strained Germanium on Silicon for Photonic Devices", ACS Applied Materials & Interfaces 7, 26470–26481 (2015).